Applied Catalysis B: Environmental 246 (2019) 356–366

Contents lists available at ScienceDirect

Applied Catalysis B: Environmental

journal homepage: www.elsevier.com/locate/apcatb

Ag-incorporated macroporous CeO_2 catalysts for soot oxidation: Effects of Ag amount on the generation of active oxygen species

Jae Hwan Lee[a], Seong Ho Lee[a,b], Jin Woo Choung[c], Chang Hwan Kim[c], Kwan-Young Lee[a,b,*]

[a] Department of Chemical and Biological Engineering, Korea University, 145, Anam-Ro, Seongbuk-Gu, Seoul, 02841, Republic of Korea
[b] Super Ultra Low Energy and Emission Vehicle (SULEEV) Center, Korea University, 145, Anam-Ro, Seongbuk-Gu, Seoul, 02841, Republic of Korea
[c] Advanced Catalysts and Emission-Control Research Lab, Research & Development Division, Hyundai Motor Group, Hyundaiyeonguso-Ro, Namyang-Eup, Hwaseong-Si, Gyeonggi-Do, 18280, Republic of Korea

ARTICLE INFO

Keywords:
Soot oxidation
Macroporous structure
Ag-loaded CeO_2
Surface oxygen vacancies
Active oxygen species

ABSTRACT

A series of CeO_2-based catalysts were investigated for soot oxidation with O_2. The macroporous CeO_2 catalyst (M-CeO_2) showed higher soot oxidation activity than mesoporous CeO_2 due to the enhanced contact between catalyst and soot caused by the large pore size of M-CeO_2. Moreover, various amounts of Ag (2–20 wt.%) were introduced to M-CeO_2 to increase the activity, and the Ag-incorporated macroporous CeO_2 catalysts (Ag(x)_M-CeO_2) were characterized. Raman spectra showed that the ratio of active oxygen species (O_x^{n-}) were different according to amount of Ag. The ratio of highly reactive superoxide (O_2^-) was largest for the Ag(5)_M-CeO_2 catalyst, and then it was decreased as the Ag amount increased further. In addition, XPS analysis showed that the difference in O_x^{n-} generation could be attributed to diverse surface oxygen vacancies in the catalysts. Hence, the amount of loaded Ag affected the surface oxygen vacancies of Ag(x)_M-CeO_2 and consequently the ratio of O_x^{n-} was different according to the surface oxygen vacancies of the catalysts. Ag(5)_M-CeO_2 with the appropriate surface oxygen vacancies induced the promotion of O_2^- generation, resulting in the best soot oxidation activity. It was concluded that the amount of Ag on CeO_2 has a great influence on the catalytic soot oxidation activity, and proper surface oxygen vacancies facilitated O_2^- generation, whereas excessive surface oxygen vacancies hindered the formation of highly reactive O_x^{n-}.

1. Introduction

Recently, regulations of automobile emissions have been continuously strengthened, and diesel vehicles are regulated to reduce various pollutants such as NO_x, CO, hydrocarbons, and soot in exhaust gases [1–7]. Soot (small-size carbon particles), a hazardous material, is primarily generated by incomplete fuel combustion and is removed by the diesel particulate filter (DPF) in the purification system. Since the soot could be stacked in the DPF, it should be continuously oxidized and removed from the filter by the purification system to maintain optimal filtration ability [4,8]. Therefore, several kinds of oxidation catalysts for the DPF have been studied to improve combustion efficiency by thinly coating an oxidation catalyst on the filter. Many studies have reported that CeO_2-based catalysts, which are used for various oxidation reactions, have remarkable activity for soot oxidation due to their ability to switch between Ce^{3+} and Ce^{4+} states resulting in high oxygen storage capacity (OSC) performance [9–12]. Hence, CeO_2 could store O_2 in an oxidizing atmosphere and release it in reduction conditions due to the OSC and redox properties [9,10].

In the soot oxidation using a CeO_2 catalyst, the reduction of the CeO_2 lattice oxygen leads to the formation of vacant sites which are then filled with gaseous O_2 [13]. Since a redox cycle of CeO_2 occurs during the soot oxidation, it has been known that the OSC and redox properties of CeO_2 are important for soot oxidation [14–17]. In contrast, several studies proposed that the bulk OSC of CeO_2 is not crucial factor, but the generation of active oxygen and transfer to soot is rather more important for the soot oxidation activity [9,16,18,19] implying that the active oxygen species (O_x^{n-}) could exist as peroxide (O^-) or superoxide (O_2^-). Machida et al. suggested that the reactive oxygen (O_2^-) formed from gas phase O_2 is adsorbed at the three-phase boundary between soot, reduced CeO_2, and the gas phase [9]. In addition, Liu et al. reported that O_2 is adsorbed on the CeO_2 surface and the various O_x^{n-} species are continuously consumed and generated on ceria surface through the following consecutive reduction of oxygen by CeO_2 surface oxygen vacancies [20]: (i) O_2 may migrate to the ceria surface which is in contact with soot and (ii) converted into O_x^{n-} simultaneously through several electronic states by reduction, which is $O_2 \rightarrow O_2^- \rightarrow 2O^- \rightarrow O^{2-}$ [20,21]. Among the various oxygen species,

* Corresponding author at: Department of Chemical and Biological Engineering, Korea University, 145, Anam-Ro, Seongbuk-Gu, Seoul, 02841, Republic of Korea.
E-mail address: kylee@korea.ac.kr (K.-Y. Lee).

https://doi.org/10.1016/j.apcatb.2019.01.064
Received 21 November 2018; Received in revised form 18 January 2019; Accepted 23 January 2019
Available online 23 January 2019
0926-3373/

O_2^- has higher activity than O^- and O^{2-} species for soot oxidation [9,21–23]. Hence, the vacancies in CeO_2 promote the migration of bulk oxygen towards the reaction site, and CeO_2 needs to have sufficient surface oxygen vacancies to promote the generation of active oxygen species (O_x^{n-}). However, the excessive surface oxygen vacancies could induce the generation of less active oxygen species. Wang et al. reported that excessive surface oxygen vacancies can lead to the formation of less active species (like O^{2-}) rather than O_2^-, which results in decrease of the catalysts' redox stability and activity [21]. In contrast, if the concentration of surface oxygen vacancies is too low, the total O_x^{n-} generation process will be hindered resulting in a slowed reaction [20,21]. Consequently, to improve soot oxidation activity, it is important to have a high proportion of O_2^- in the successive O_2 reduction steps, and this requires an appropriate amount of surface oxygen vacancies.

Ag metal has been known to remarkably promote the formation of O_2^- oxygen species and the supplementation of active oxygen [9,22,24–26]. The atomic oxygen is reduced by surface oxygen vacancies and in this process, Ag has been proven effective for gaseous O_2 dissociation and CeO_2 bulk oxygen utilization, improving the O_2^-, O^-, and O^{2-} generation of the Ag/CeO_2 and resulting in enhanced soot oxidation activity. Therefore, the ratio of active O_x^{n-} species (O^-, O^{2-} and especially O_2^-) on the ceria surface is one of the most important factors responsible for soot oxidation over Ag-loaded CeO_2 [10,21,27]. Meanwhile, a few studies have been conducted on the difference in activity of CeO_2 in soot oxidation depending on the amount of Ag. Aneggi et al. reported that lower oxidation temperatures were found between 5 wt.% and 10 wt.% loading of Ag for CeO_2, ZrO_2, and Al_2O_3 supports [24]. Additionally, the onset temperature of soot oxidation can be lowered as the amount of Ag on CeO_2 increases [9], and the T_{max} for soot oxidation as a function of the Ag amount in the Ag/CeO_2 catalysts were reported [26]. However, to the best of our knowledge, the explanations on the difference in activity of various amounts of Ag-loaded CeO_2 due to correlations between surface oxygen vacancies with the generation of active oxygen species have not been reported. There should be an appropriate amount of Ag on the CeO_2 and surface oxygen vacancies concentration that optimizes the activity and formation rate of O_x^{n-}. In this work, to solve the above issues, as well as to improve the ceria-soot contact, macroporous structured CeO_2 was chosen as a support since the macroporous structure catalysts indicated improved soot oxidation efficiency due to enhanced ceria-soot contact [17,28–30]. Prior to this study, Ag-loaded macroporous CeO_2 catalysts have not yet been applied to soot oxidation; thus, herein, Ag-loaded macroporous CeO_2 catalysts were applied to the soot oxidation reaction in this study.

Based on the macroporous CeO_2 (M-CeO_2), a series of Ag-loaded M-CeO_2 catalysts (Ag(x)_M-CeO_2) with similar morphologies and different Ag loadings were synthesized and examined. Through characterization and comparison of the activity of the catalysts for soot oxidation, the appropriate amount of active oxygen species and surface oxygen vacancies for a given amount of Ag were verified. The results suggest a correlation between the optimum amount of Ag and the surface oxygen vacancies of CeO_2, resulting in active oxygen species generation and activity improvement.

2. Experimental

2.1. Preparation of catalysts

The macroporous structure catalysts were synthesized using PMMA as templates by modifying the methods found in the literature [29,31]. A PMMA template was synthesized through a series of polymerization processes using methyl methacrylate (MMA, Sigma Aldrich) and potassium persulfate (Sigma Aldrich) as the precursors. MMA (240 ml) and deionized water (560 ml) were mixed in a 1000-ml four-neck and round-bottom flask, and 1.62 g of potassium persulfate (Sigma Aldrich) was added to the solution. After the mixture was heated to 70 °C, the solution was rotated by a motor stirrer under an Ar gas flow condition. With a constant stirring rate (400 rpm), the mixture was kept at 70 °C for 2 h. After the reaction was finished, the homogeneous PMMA template was obtained by centrifugation. By using a centrifuge, the mixed solution was packed into colloidal crystals, and then, the template was dried at 60 °C overnight.

Cerium nitrate hexahydrate ($Ce(NO_3)_3{\cdot}6H_2O$, Sigma Aldrich) was used as precursor to synthesize the CeO_2 catalysts. A total of 15 ml of ethylene glycol (Sigma Aldrich) and 10 ml of methanol (Sigma Aldrich) were mixed (60 vol.% of ethylene glycol) and 21.7 g of cerium precursor was dissolved into 25 ml of the solution. Then, the mixture was stirred in a 100 ml beaker at room temperature for 2 h and added to the prepared PMMA template for 4 h. Excessive liquid was removed using Buchner funnel connected vacuum. The infiltered template was dried and calcined with quartz sand (Sigma Aldrich) at the rate of 1 °C/min from room temperature to 550 °C in air (200 ml/min) in a quartz tube for 5 h to remove the PMMA template. The CeO_2 catalyst prepared using above method was denoted as M-CeO_2 catalyst. For comparison, a mesoporous CeO_2 catalyst was also synthesized by the calcination of Ce $(NO_3)_3{\cdot}6H_2O$ at 550 °C for 5 h and denoted as m-CeO_2.

In addition, Ag-loaded M-CeO_2 catalysts were synthesized using silver nitrate ($AgNO_3$) precursor obtained from Sigma Aldrich. In the process of the M-CeO_2 catalyst synthesis, a certain amount of $AgNO_3$ was added to a mixture of ethylene glycol and methanol to incorporate 2, 5, 10, and 20 wt.% of Ag on M-CeO_2. Then, the PMMA template was introduced to the solution, and the remaining parts of the method were performed as described above. The prepared Ag-loaded M-CeO_2 catalysts were denoted as Ag(x)_M-CeO_2 (x = 2, 5, 10, 20) according to Ag wt.% amounts.

2.2. Characterizations

The mass fractions of Ag in the Ag(x)_M-CeO_2 catalysts were estimated by inductively coupled plasma atomic emission spectroscopy (ICP-AES) using a JY Ultima2C (Jobin Yvon) at the Korea Basic Science Institute (Seoul Branch).

High-resolution scanning electron microscopy (HRSEM) analysis was performed using a Hitachi SU-70 at the Korea Basic Science Institute (Seoul Branch) to investigate the morphology of several samples. Additionally, energy dispersive spectrometry (EDS) analysis was conducted to verify the distribution of elements in each sample. Before SEM and EDS analysis, the samples were coated with Pt beam to increase electron conductivity.

Through high-resolution transmission electron microscopy (HRTEM), the contact between soot and catalysts was verified, and EDS elements mapping images of Ag-loaded catalysts were taken to examine the Ag metal dispersion over CeO_2. The samples were dispersed in ethanol, dropped on 300 mesh carbon coated grids and then dried before measurements. Analyses were performed by HRTEM (Titan themis3 Double Cs & Mono. TEM at 300 kV) at the Korea Basic Science Institute (KBSI) in Seoul.

N_2 adsorption-desorption analysis was conducted at −196 °C using a BELSORP-max instrument (BEL Japan Inc.). The surface area was calculated using the BET equation and pore diameter was estimated with the BJH method.

Powder X-ray diffraction (XRD) patterns were recorded by a diffractometer (Rigaku SmartLab) through Cu Kα (λ = 1.5406 Å) irradiation. The analysis was conducted in the 2θ range of 10° to 85° with a scanning rate of 2°/min.

H_2-temperature programmed reduction (H_2-TPR) analyses were carried out on an AutoChem II 2920 instrument (Micromeritics). The sample (50 mg) was placed in a quartz tube, which was purged with He (50 ml/min) for 30 min at 200 °C. H_2-TPR data of the prepared sample were recorded upon raising the temperature from 50 °C to 900 °C in a flow of 10% H_2/Ar (50 ml/min) with a heating rate of 5 °C/min.

Raman spectra were acquired with a LabRAM ARAMIS IR2 (HORIBA Jobin Yvon) analyzer at room temperature. A wavelength of 532 nm was used for the exciting source and the spectra were taken from 700 to 1600 cm^{-1}.

X-ray photoelectron spectroscopy (XPS) experiments were carried on a PHI 5000 VersaProbe with an Al Kα X-ray source (1486.6 eV), and the binding energies were calibrated with the reference of C1 s binding energy at 284.6 eV. The core electrons of Ce 3d, Ag $3d_{5/2}$ and O 1s were investigated.

2.3. Activity test of catalyst

Printex U (Degussa) was used as the model material for soot in this study. The properties of Printex U have been known from several studies in the past, and the particle diameter is more than approximately 20 nm [20,32,33]. The activity tests of the prepared catalysts in soot oxidation were performed using a temperature programmed oxidation (TPO) instrument. Tests were carried out in a fixed-bed reactor (a quartz tube, with an inner diameter of 7 mm, heated by an electric). A thermocouple was placed as close as possible to the catalytic bed, still not being in direct contact. The oxidizing atmosphere mixture with 20 vol.% of O_2 in He, 10 vol.% of O_2 in He, and 5 vol.% of O_2 in He, respectively, was fed at a constant rate of 100 ml/min to the reactor with H_2O (5 vol.%). The catalytic bed was prepared by mixing 2 mg of Printex U and 20 mg of the prepared catalysts using spatula for 5 min (loose contact). The reaction temperature was programmed to increase to 800 °C with 5 °C/min heating rate, and CO_2 concentration in the reactor outlet was measured in FT-IR analyzers (Nicolet is50, ThermoFisher Scientific). The temperature corresponding to the highest concentration of CO_2 was denoted as T_m for the activity tests, and the temperatures corresponding to the point where 20% and 50% of the soot were combusted were denoted as T_{20} and T_{50}, respectively. In addition, isothermal reaction tests were performed to verify the catalytic activity using the TPO instrument. The soot and catalyst were mixed with loose contact and the mixture was heated to 450 °C and 500 °C, respectively, under a He flow condition. Then, the oxidation reaction was initiated by flowing the 80 ml/min of He and 20 ml/min of O_2 with H_2O (5 vol.%), and the isothermal condition was maintained. The times required for 20% and 50% of the soot to be combusted in the isothermal tests were denoted as t_{20} and t_{50}, respectively.

3. Results and discussion

3.1. Textural properties of the samples

The morphology and pore structure of the samples were examined by high-resolution scanning electron microscopy (HRSEM). Fig. 1a shows SEM image of Printex U and the image demonstrates that the Printex U particle size is larger than approximately 20 nm and varied from 20 nm to 150 nm since it is not uniform size and could agglomerate with other particles. Due to this large particle combination, it could be difficult for soot to migrate into inner pores of catalysts with small pore diameters. Fig. 1b is SEM image of m-CeO_2, and the morphology and pore structure of m-CeO_2 are extremely amorphous and the pore size is small in the micro- and mesopore range, which verifies that the particle size of Printex U is usually larger than the pore size of m-CeO_2.

Additionally, Fig. 1c and d are SEM images of the synthesized PMMA template with different magnifications and the evaluated PMMA particle size is uniformly 350–370 nm. Fig. 1e and f are SEM images of the prepared M-CeO_2 catalyst with different magnifications and the pore sizes of M-CeO_2 estimated from the SEM image are 250–300 nm, which corresponds to a slight shrinkage from the initial PMMA particle size. The pore sizes of M-CeO_2 are clearly larger than that of m-CeO_2, and it is more advantageous structure for soot to penetrate into pores of CeO_2. After Ag impregnation, the pore structure and morphology of the catalysts show no obvious structure change, and thus it, the structure change due to the deposition effect of Ag may be negligible (Fig. 1g). The loaded Ag particle and Ce dispersion of Ag(5)_M-CeO_2 could be verified by energy dispersion spectrometer (EDS) mapping (Fig. 1h, i, j). The EDS analysis results show that loaded Ag and Ce are well dispersed along the CeO_2 frame structure in Ag(5)_M-CeO_2 catalysts. The results indicate that the overall structure and pore sizes of Ag(5)_M-CeO_2 catalysts are similar to the M-CeO_2 catalyst and that Ag metals are evenly dispersed on the surface.

The contact between soot and the catalysts could be different depending on the catalyst morphologies, and the soot-catalyst contact has a great influence on the activity. Hence, the mixture of soot and catalyst after loose contact was verified through HRSEM. In Fig. 2a and b, the mixture of soot and m-CeO_2 is represented with different magnifications, and the aggregated soot is mainly attached to the surface of CeO_2 since the pore size of CeO_2 is not large enough. On the other hand, the mixture of soot and M-CeO_2 indicates considerably different contact, and soot is distributed in the large pores of the catalyst (Fig. 2c and d). In addition, high-resolution transmission electron microscopy (HRTEM) was applied to confirm the contact between soot and the catalysts, and the results are represented in Fig. 2e and f. The agglomerated soot can hardly penetrate into the mesopore of m-CeO_2 [16], and the contact between soot and inner pore of m-CeO_2 is difficult to occur (Fig. 2e). On the other hand, the soot is present in the macropore of M-CeO_2 and has relatively more efficient contacts with the catalyst (Fig. 2f). Consequently, M-CeO_2 indicates more suitable contact in large pores of macroporous structure, in which the soot could enter more easily.

HRTEM was applied to analyze the particle size of Ag loaded on macroporous CeO_2 and the EDS mapping analysis results are shown in Fig. 3. The loaded Ag forms particles and is dispersed over CeO_2. The particle sizes of Ag over the catalysts were estimated using EDS mapping results. Although the amounts of Ag particle increase, the size of the Ag particles is not significantly different, and the average size is about 6 nm (Table 1). In addition, the dispersion of Ag on CeO_2 based on ICP results were calculated according to reported methods [34] and are listed in Table 1. As a result, regardless of the amount of Ag, Ag particle is uniformly well dispersed and there is no significant difference in Ag dispersion (19–21%).

The BET surface area and pore diameter of the samples are summarized in Table 1, and The N_2 adsorption-desorption isotherms of the catalysts are shown in Fig. 4a. The BET surface area of m-CeO_2 (79.2 m^2/g) is higher than the surface area of M-CeO_2 due to the mesoporous structure with a small pore diameter of 9.4 nm (Table 1). In contrast, M-CeO_2 has a very low surface area (12.7 m^2/g) due to macroporous structure and large pore diameter, implying a significant morphological difference between m-CeO_2 and M-CeO_2. As shown in the SEM and TEM images of the soot-catalyst mixture (Fig. 2), it is important that the catalyst has a pore size that allows the soot particles to easily pass through and contact with the inner pore of CeO_2 [29,30,32]. Meanwhile, the surface areas of Ag-impregnated catalysts (11.7–13.8 m^2/g) are similar to that of M-CeO_2 regardless of Ag amount, and thus, the surface area change after Ag loading is negligible. In Fig. 4a, the M-CeO_2 and Ag(x)_M-CeO_2 catalysts indicated a type II nitrogen adsorption curve. The low relative pressure (p/p_0) range indicates near linear section of the isotherm, which suggests that the catalysts are nonporous or macroporous structure [35]. On the other hand, the hysteresis loop in the range of high relative pressure represents that the pore walls of the macroporous catalysts have mesopores within the wall [36]. Hence, the M-CeO_2 and Ag(x)_M-CeO_2 catalysts have similar macroporous structure and possess micro-mesopores in the wall of the catalysts.

Fig. 4b presents XRD spectra obtained from the prepared samples. The spectrum of M-CeO_2 catalyst shows fluorite phase peaks, and these findings are consistent with reported results of CeO_2 XRD spectra [2,20,37]. In the case of Ag-loaded catalysts, the signals derived from metallic Ag are mainly existed at $2\theta = 38.08°$, 44.21° and 64.35°, etc. [2,38], which are invisible in Ag(2)_M-CeO_2 due to the small amount of Ag. The metallic Ag peaks are visible for Ag(x)_M-CeO_2 catalysts with 5 wt.% Ag or more, and the larger and more obvious Ag metallic peaks appeared as Ag loading amounts increased. Additionally, it should be

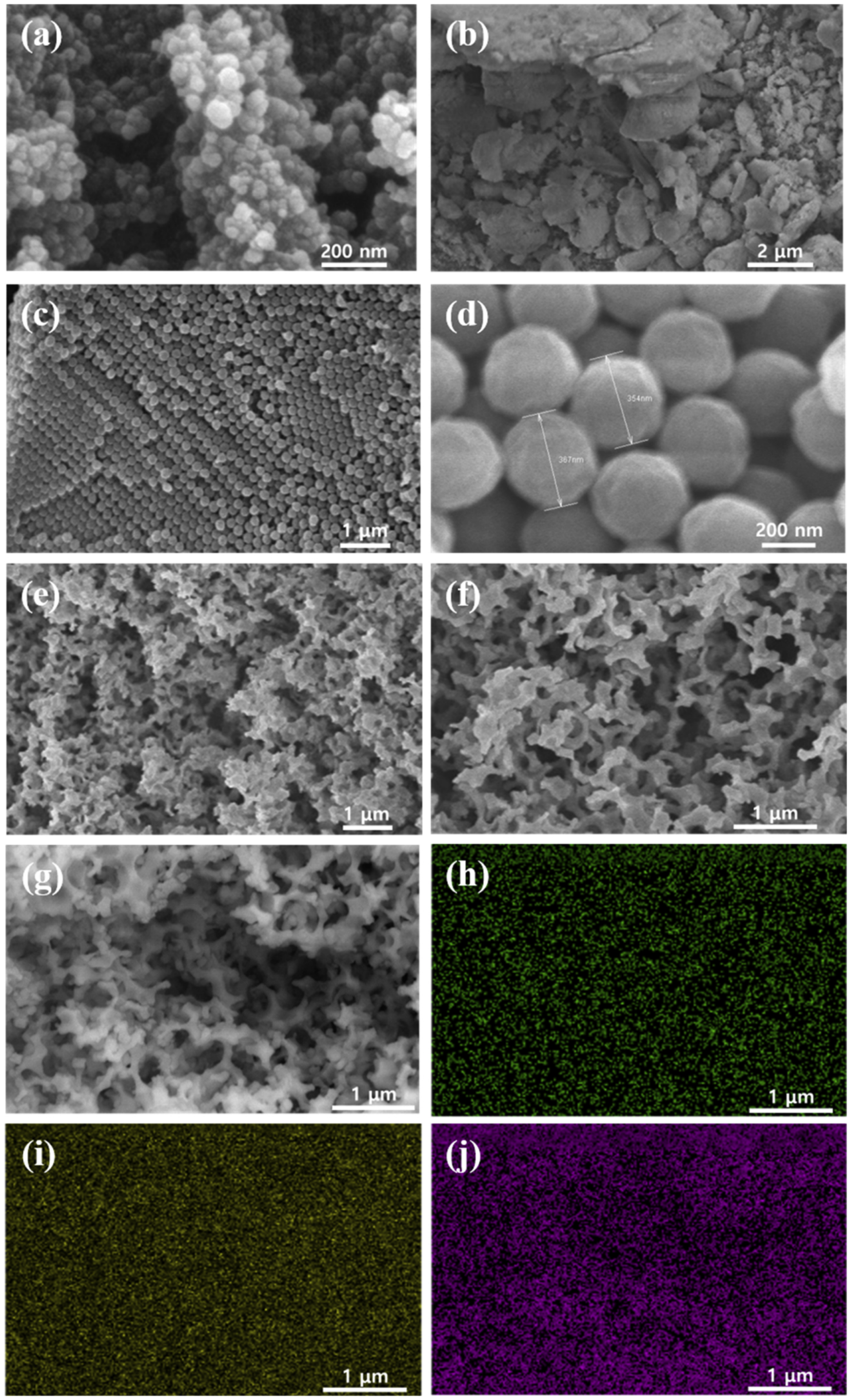

Fig. 1. SEM images of (a) Printex U, (b) m-CeO_2, (c, d) PMMA with different magnifications, (e, f) M-CeO_2 with different magnifications, (g) Ag(5)_M-CeO_2, and (h, i, j) EDS analysis results of Ag(5)_M-CeO_2. ((h) Ag, (i) Ce, and (j) O).

noted that the loaded Ag metal mainly presented as Ag^0 (metallic) state since the $Ag^{\delta+}$ peaks are hardly visible. According to S. Liu et al., Ag may exist as a metallic state when Ag is loaded on CeO_2 [20], and in agreement with this, Ag appears to exist in a metallic state in the XRD results (Fig. 4b). In contrast, some studies have shown that Ag_2O crystallites peak may also be present in the XRD pattern of Ag-loaded CeO_2 catalyst [2,39]. Hence, the coexistence of Ag metallic peak and AgO_x peak needs to be investigated thoroughly. As a result of expanding the peak of Ag(20)_M-CeO_2 catalyst at $2\theta = 38.08°$ (Fig. 4c), a small peak (shouldering) attributed to Ag_2O at $2\theta = 37.86°$ also appeared to exist, but it was not enough to distinguish it from the Ag peak at $2\theta = 38.08°$. It has been known that the diffraction lines corresponding to the Ag_2O structure have relative low intensities at 2θ values close to the cerianite diffraction lines which made its identification difficult [2], and this dynamic might be due to the high dispersion of the Ag particles over the CeO_2. Therefore, to identify the possibility of the existence of Ag^0 and $Ag^{\delta+}$ states, H_2-TPR and XPS analysis were additionally carried out on the prepared samples alongside the XRD analysis.

3.2. Catalytic activity test for soot oxidation

Fig. 5 and Table 2 show the activity test results of the prepared

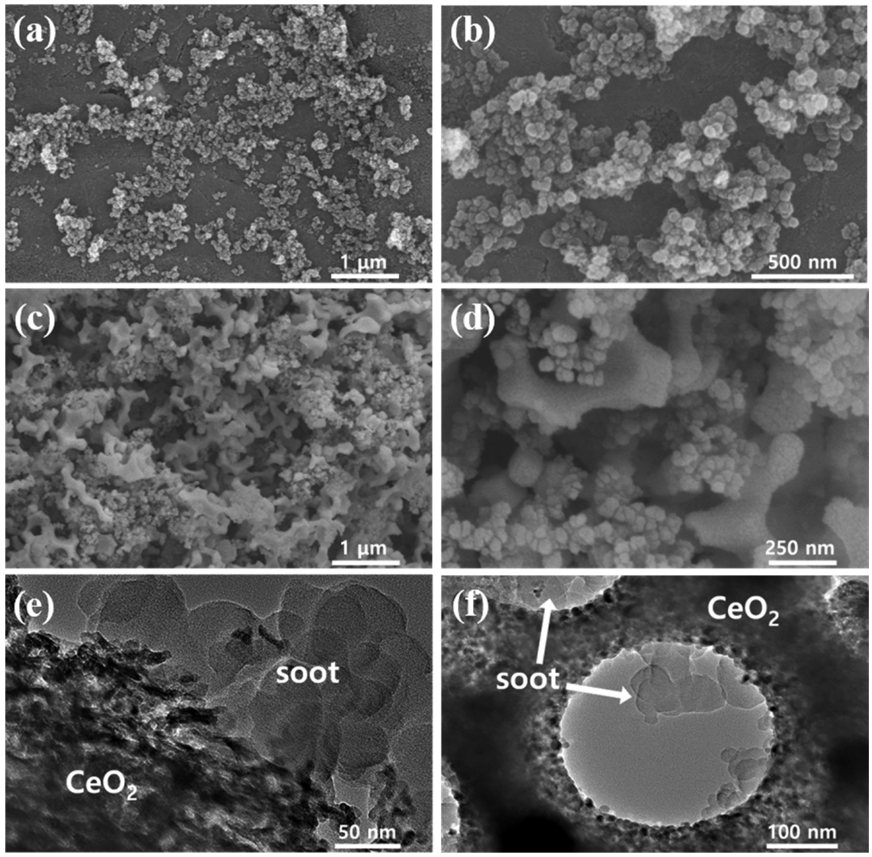

Fig. 2. SEM images of (a, b) soot + m-CeO_2 mixture, (c, d) soot + M-CeO_2 mixture with different magnifications, TEM images of (e) soot + m-CeO_2 contact, and (f) soot + M-CeO_2 contact.

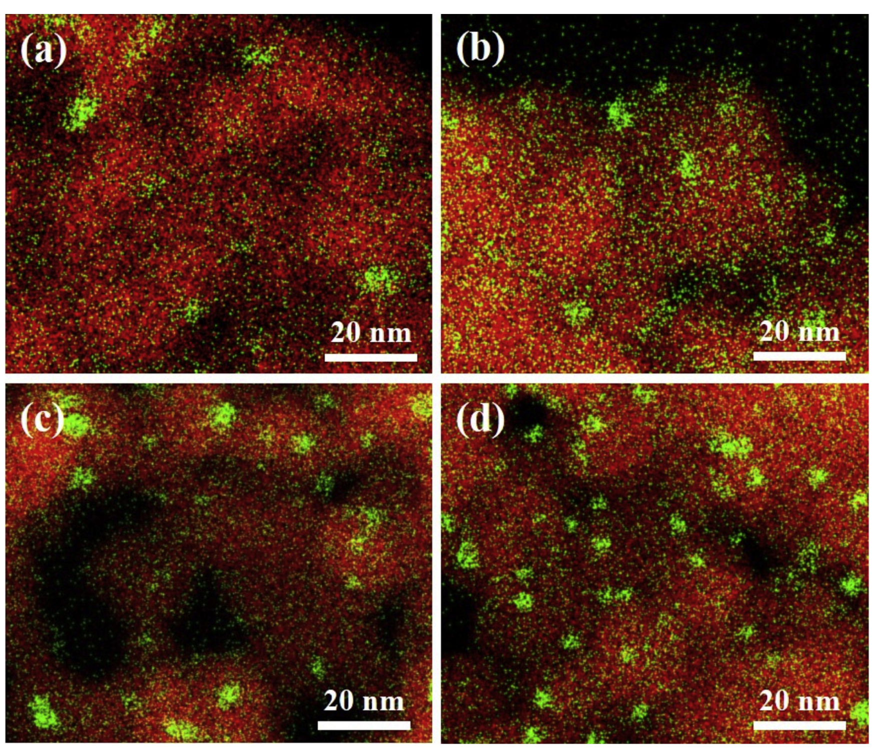

Fig. 3. EDS mapping results (HRTEM) of (a) Ag(2)_M-CeO_2, (b) Ag(5)_M-CeO_2, (c) Ag(10)_M-CeO_2, and (d) Ag(20)_M-CeO_2.

catalysts. The T_{20} and T_{50} of the soot oxidation tests with H_2O were shown in Fig. 5, and the results are summarized in Table 2. Printex U oxidation without catalyst indicated T_{20} at 498 °C and T_{50} at 560 °C. For the CeO_2 catalysts, m-CeO_2 catalyst showed improved activity, and especially, M-CeO_2 catalyst indicated higher activity than m-CeO_2 catalyst. This is because the soot could migrate to the inner pore easily and

Table 1
The Ag content and properties of the prepared samples.

Sample	Ag content (wt. %)[a]	Ag particle size (nm)[b]	Ag dispersion (%)	BET surface area (m^2/g)[c]	Pore diameter (nm)	Surface Ce^{3+}/Ce^{4+} ratio[e]	$[O_V]/([O_V]+[O_L])$[e]
m-CeO_2	–	–	–	79.2	9.4[c]	–	–
M-CeO_2	–	–	–	12.7	250–300[d]	0.55	0.45
Ag(2)_M-CeO_2	1.7	6.1	19	13.2		0.31	0.25
Ag(5)_M-CeO_2	4.8	5.9	21	12.1		0.15	0.21
Ag(10)_M-CeO_2	9.8	5.8	21	11.7		0.20	0.38
Ag(20)_M-CeO_2	16.1	5.6	21	13.8		0.23	0.41

[a] Obtained from the ICP-AES.
[b] Estimated from the HR-TEM.
[c] Obtained from N_2 physisorption at −196 °C.
[d] Evaluated by SEM images.
[e] Calculated by the XPS data.

the contact between soot and catalyst is enhanced. The macroporous structure was favored for soot oxidation since the particle size of the soot was larger than approximately 20 nm and the small pore sizes of the catalyst could limit the entry and transport of soot particles into the inner pore of the catalyst [29,30].

After Ag impregnation, the Ag-loaded catalysts have the improved catalytic activity for soot oxidation and lower T_m temperature than pure M-CeO_2 under different vol.% of O_2 flow conditions (Fig. 6a, b, and c). Especially, Ag(5)_M-CeO_2 indicated the lowest T_m among the Ag(x)_M-CeO_2 catalysts under the conditions of each O_2 concentration. On the other hand, the activity of the catalysts decreased with an Ag amount more than 5 wt.% in the reaction conditions. In Fig. 6d, the T_m of the catalysts are compared under different O_2 concentrations, and the order of catalytic activity in each reaction condition was the same. The activity of M-CeO_2 decreased significantly under lower O_2 contents, whereas the activity of each Ag(x)_M-CeO_2 catalyst was maintained or slightly decreased as the vol.% of O_2 decreased. Hence, an amount of 5 wt.% of Ag is considered to be the optimized Ag amount between 2–20 wt.% contents, and the activity of the catalysts based on T_m follows the order Ag(5)_M-CeO_2 > Ag(10)_M-CeO_2 > Ag(2)_M-CeO_2 > Ag(20)_M-CeO_2 > M-CeO_2.

In addition, the isothermal activity tests were performed to verify the ability of the catalysts in soot oxidation. In isothermal conditions, the soot oxidation reactions were carried out at suitable temperatures to examine the difference in activity. The mixture of soot and catalyst by loose contact was heated to 450 °C and 500 °C, respectively, at which the oxidation of soot is relatively slow to clearly distinguish the difference in activity. Then, the oxidation was initiated, and the time required to combust the soot at each temperature was recorded. The t_{20} and t_{50} values of each mixture samples were attained and the results are illustrated in Fig. 7. In Fig. 7a, all Ag-loaded catalysts showed a much faster soot oxidation rate than M-CeO_2 at 500 °C, and in particular, the t_{50} for the M-CeO_2 catalyst was larger than that of other catalysts. In addition, Ag(5)_M-CeO_2 catalyst indicated the fastest soot oxidation rate followed by Ag(10)_M-CeO_2, Ag(2)_M-CeO_2, and Ag(20)_M-CeO_2, respectively (Fig. 7b). Even at the isothermal temperature of 450 °C, Ag(5)_M-CeO_2 showed the fastest oxidation rate among the catalysts. Although t_{20} and t_{50} values were increased due to lower temperature, the order of the catalysts was the same as that of the 500 °C isothermal condition (Fig. 7c and 7d). Therefore, the proper amount of Ag impregnation to CeO_2 resulted in improved soot oxidation ability in both heating and the isothermal tests, and Ag(5)_M-CeO_2 indicated the largest improvement in activity.

The soot oxidation activity depending on the amount of Ag on CeO_2 has been studied in a few reported studies and the lower oxidation temperatures were found according to Ag amount [9,24,26]. However, the explanation of the difference in activity due to various amounts of Ag and the correlations between surface oxygen vacancies with the generation of active oxygen species (O_x^{n-}) have not been reported. Additionally, an optimum amount of Ag on the macroporous CeO_2 needs to be investigated in terms of active oxygen species effect on soot oxidation.

3.3. Reducibility of the samples

Fig. 8 shows H_2-TPR profiles of the M-CeO_2 and Ag(x)_M-CeO_2 catalysts. In the 50–900 °C temperature region, the M-CeO_2 catalyst shows two major reduction peaks at approximately 500 °C and 690 °C, respectively. The reduction peak at lower temperature could be attributed to the reduction of surface oxygen of CeO_2, and the other peak at higher temperatures could be the reduction of the bulk oxygen of CeO_2 [15,16,39–41]. For Ag-loaded catalysts, the reduction of surface active oxygen at 500 °C shifts to a lower temperature by approximately 60 °C and the size of peak largely decreases, whereas the reduction behavior of bulk oxygen slightly shifted by approximately 15–25 °C.

Meanwhile, Ag(x)_M-CeO_2 catalysts indicate one additional peak at from 167 °C to 222 °C. The Ag(2)_M-CeO_2 and Ag(5)_M-CeO_2 catalysts show small peak at approximately 220 °C and broad peaks of similar size. On the other hand, Ag(10)_M-CeO_2 catalyst shows a larger peak shifted to a lower temperature at 205 °C. The Ag(20)_M-CeO_2 catalyst represents a clearly shifted peak at 167 °C, and the size of the peak is much larger than that of other Ag(x)_M-CeO_2 catalysts. Considering that Ag^0 and Ag^+ may coexist in Ag(x)_M-CeO_2 catalysts, the added reduction peaks could be attributed to the reduction of silver oxides [37,42], and the size of peaks are varied according to amount of Ag. In addition, it has been reported that the presence of Ag would weaken the Ce-O bond adjacent to silver species and improve the reducibility of surface oxygen on CeO_2 [39,43,44]. Therefore, these additional peaks at lower temperature also could be due to the reduction of surface oxygen of CeO_2 interacting with silver species. Consequently, for Ag(x)_M-CeO_2 catalysts, the reduction peaks at 167–222 °C are attributed not only to the reduction of silver oxides but also to the reduction of surface oxygen of ceria interacting with silver species, and the sizes of peak are varied according to amount of silver species. Moreover, the reduction peaks at 435 °C attributed to the surface oxygen of ceria away from silver species became largely small, and the reduction temperature of bulk oxygen of CeO_2 was relatively less affected.

Generally, when the reduction of surface active oxygen species occurs at a lower temperature, the reducibility of the catalyst increases and the activity for oxidation process is improved. From the results of catalytic activity test, it was determined that the dissociation of oxygen and the generation of active oxygen species were improved by Ag incorporation. However, as the amount of Ag was increased, the activity did not increase continuously, and this is probably because excessive amounts of Ag existed as $Ag^{\delta+}$ state, which is an Ag species that might have little effect on the increase in catalytic activity. Hence, Ag incorporation is efficient until the optimum amount, and when it is excessive, it becomes less effective and the Ag may exist in the Ag^+ state and have little effect on the activity improvement of the Ag(x)_M-CeO_2 catalysts.

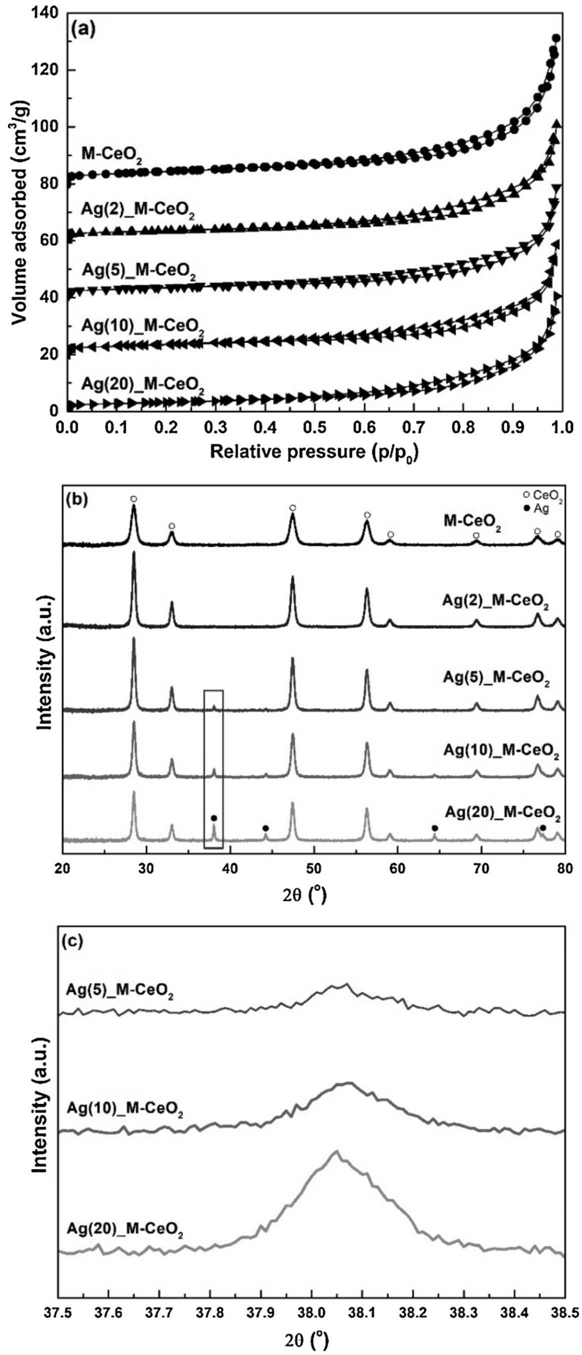

Fig. 4. (a) N_2 adsorption-desorption isotherms, (b) XRD patterns, and (c) magnified XRD patterns (2θ: 37.5–38.5°) of the $M\text{-}CeO_2$ and Ag(x)_$M\text{-}CeO_2$ catalysts.

3.4. Active oxygen species analysis of the samples

In the oxidation reaction over the CeO_2 catalyst, after O_2 is adsorbed on CeO_2 surface, the various O_x^{n-} species are continuously consumed and generated on the CeO_2 surface. O_2 may migrate to the CeO_2 surface, which is in contact with soot, and simultaneously transform into O_x^{n-} through several different electronic states, which are $O_2 \rightarrow O_2^- \rightarrow 2O^- \rightarrow O^{2-}$ [20]. Ag metal could promote the formation of O_2^-, which has higher level of activity for soot oxidation than O^- and O^{2-} species [21]. Therefore, the ratio of active O_x^{n-} species on the CeO_2 surface is crucial for Ag-loaded CeO_2. The active oxygen species of the prepared catalysts were investigated through Raman analysis to verify the catalytic performances. Raman spectra of $M\text{-}CeO_2$ and Ag(x)_$M\text{-}CeO_2$ catalysts were

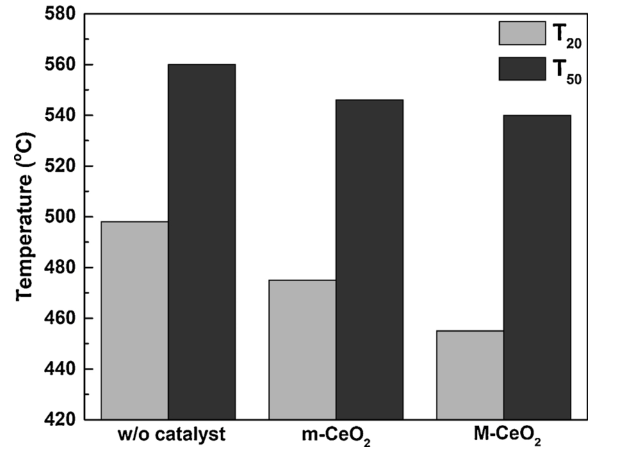

Fig. 5. The performance of soot oxidation over $m\text{-}CeO_2$ and $M\text{-}CeO_2$ under loose contact. Reaction conditions: He (80 ml min^{-1}), O_2 (20 ml min^{-1}), H_2O (5 vol.%), catalyst/soot = 10/1, heating rate = 5 °C min^{-1}.

Table 2
Soot oxidation test results of the prepared samples (°C).

Sample	T_{20} [a]	T_{50} [b]
w/o catalyst	498	560
$m\text{-}CeO_2$	475	546
$M\text{-}CeO_2$	455	540

[a] Temperature at which 20% of the soot is combusted.
[b] Temperature at which 50% of the soot is combusted.

examined and the results are shown in Fig. 9. Specifically, the bands in the ranges of 1500 and 1135–1126 cm^{-1} can be attributed to superoxide (O_2^-) whereas the peroxide species (O^-) shows bands at 964 and 883–825 cm^{-1}. The quantitative interpretation of the Raman spectra was conducted by using the intensity of the band at 1174 cm^{-1} [20,21,45,46].

With Ag participation, the bands attributed to the O_2^-, O^-, and O^{2-} increased overall when compared to $M\text{-}CeO_2$. When comparing Ag-loaded catalysts, the Ag(5)_$M\text{-}CeO_2$ catalyst and Ag(10)_$M\text{-}CeO_2$ catalyst had more O_2^- oxygen species bands in the ranges of 1130 cm^{-1} than other Ag-loaded catalysts. However, since the bands in this range were adjacent to bands of O^{2-}, the O_2^- bands at 1500 cm^{-1} of the catalyst were also compared. Ag(5)_$M\text{-}CeO_2$ catalyst showed a remarkably large peak at 1500 cm^{-1} and the Ag(5)_$M\text{-}CeO_2$ catalyst had the highest proportion of O_2^- oxygen species when compared to other catalysts. Therefore, the Ag(5)_$M\text{-}CeO_2$ catalyst exhibited higher catalytic activity than other Ag(x)_$M\text{-}CeO_2$ catalysts for soot oxidation. On the other hand, the Ag(2)_$M\text{-}CeO_2$ and Ag(20)_$M\text{-}CeO_2$ catalyst demonstrated relatively larger peaks for the peroxide species (O^-), which appeared at approximately 970 cm^{-1}, and much smaller peaks for O_2^-, subsequently resulting in lower activity in soot oxidation tests. These different ratios of active oxygen species of Ag(x)_$M\text{-}CeO_2$ caused the gap in catalytic activities for soot oxidation (Fig. 6), and the difference in active oxygen species is known to be influenced by the surface oxygen vacancies of each catalyst. As explained, O_x^{n-} was mainly generated by the formation of atomic oxygen (O) through O_2 dissociation or lattice oxygen migration, and the reduction of atomic oxygen by surface oxygen vacancies. Therefore, the surface oxygen vacancies of each catalyst should be investigated further to be correlated with the generation of active oxygen species. XPS analysis was performed to verify the surface chemical properties of the catalysts.

3.5. Electronic states and surface oxygen vacancies of samples

To examine the electronic states and surface oxygen vacancies of the samples, the synthesized $M\text{-}CeO_2$ and Ag(x)_$M\text{-}CeO_2$ catalysts were

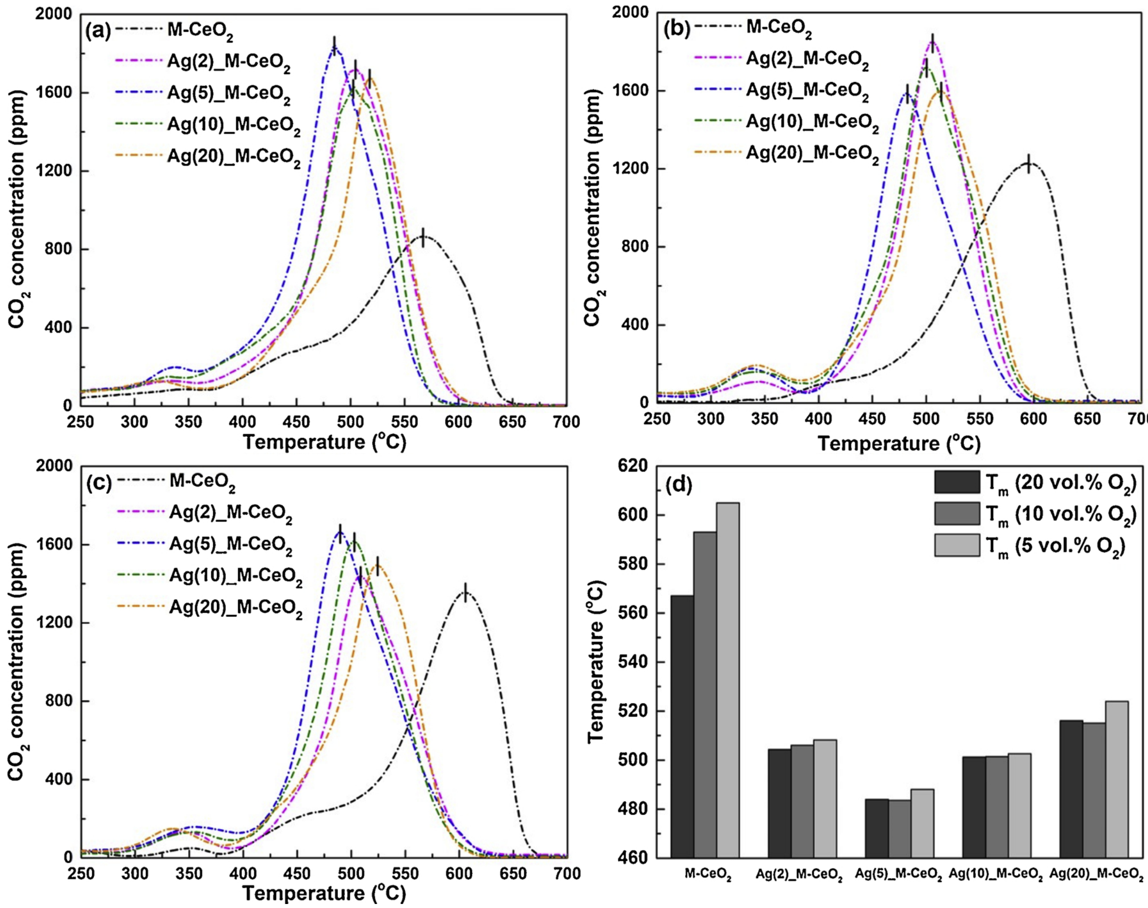

Fig. 6. The performance of soot oxidation over $M\text{-}CeO_2$ and Ag(x)_$M\text{-}CeO_2$ catalysts under loose contact. CO_2 concentration during soot oxidation under (a) 20 ml min^{-1} of O_2 and 80 ml min^{-1} of He, (b) 10 ml min^{-1} of O_2 and 90 ml min^{-1} of He, (c) 5 ml min^{-1} of O_2 and 95 ml min^{-1} of He, and (d) T_m of the catalysts under each condition. Reaction conditions: H_2O (5 vol.%), catalyst/soot = 10/1, heating rate = 5 °C min^{-1}.

analyzed by X-ray photoelectron spectroscopy (XPS), and the results are shown in Fig. 10. As shown in Fig. 10a, Ag in all Ag(x)_M-CeO_2 catalysts exhibited Ag $3d_{5/2}$ binding energies and the peak deconvolution indicated doublets in the Ag(x)_M-CeO_2 catalysts at 367.7 eV and 368.1 eV attributed to Ag^+ and Ag^0, respectively. As amount of Ag loading increased, the $Ag^{\delta+}$ peak grew larger and the Ag^0 peak decreased, implying that excessive amount of Ag induced the coexistence of Ag and AgO_x state with larger $Ag^{\delta+}/Ag^0$ ratios. These results are consistent with the XRD results (Fig. 4) and the H_2-TPR results (Fig. 8), suggesting the presence of $Ag^{\delta+}$ with Ag metallic state.

Furthermore, the spectra of the Ce 3d region and deconvoluted peaks are illustrated in Fig. 10b. The six peaks from Ce^{4+} 3d (u_{1-6}: 882.0, 888.0, 897,8. 900.5, 907.0, and 916.3 eV) and four peaks from Ce^{3+} 3d (v_{1-4}: 881.0, 884.0, 899.3, and 902.3 eV) were represented [20,27,39]. As listed in Table 1, the Ag(x)_M-CeO_2 catalysts had the various Ce^{3+}/Ce^{4+} ratios. M-CeO_2 had a higher surface Ce^{3+}/Ce^{4+} and the ratio decreased with the incorporation of Ag due to the interaction between the Ag metal and CeO_2 ($Ag^+ + Ce^{3+} \rightarrow Ag^0 + Ce^{4+}$). Therefore, this interaction over Ag/CeO_2 induced a low Ce^{3+}/Ce^{4+} and [V_O] (surface oxygen vacancies concentration) of ceria and the formation of metallic Ag [20]. In addition, the surface Ce^{3+}/Ce^{4+} ratios between Ag(x)_M-CeO_2 catalysts were varied depending on amount of Ag. The Ag(5)_M-CeO_2 indicated the lowest value for the surface Ce^{3+}/Ce^{4+} ratio among Ag(x)_M-CeO_2 catalysts while the ratio tended to increase as the Ag content exceeded 5 wt.%.

Fig. 10c is the result of an O 1s deconvolution peak from the surface oxygen of each catalyst, and the O 1s peak could be divided into O_L, O_V, and O_C peaks, which refer to O^{2-} in the lattice (O_L), O^{2-} in the oxygen vacancies (O_V), and the surface-chemisorbed oxygen species (O_C), respectively [27]. The number of surface oxygen vacancies can be evaluated from the ratio of $[O_v]/([O_v] + [O_L])$ [20], and the ratios were estimated based on the O 1s peak and are listed in Table 1. The presence of Ce^{3+} is related to surface oxygen vacancies, and [V_O] near the catalyst-soot interface may be different depending on the catalysts [21]. The incorporation of Ag decreased the [V_O] of all the Ag(x)_M-CeO_2 catalysts, which is consistent with the result from the Ce 3d spectra that showed a lower Ce^{3+}/Ce^{4+} ratio of Ag(x)_M-CeO_2 than M-CeO_2. Additionally, the Ag(5)_M-CeO_2 catalyst represented a smaller [V_O] value than the other Ag(x)_M-CeO_2 catalysts, which agrees with the result of the lowest surface Ce^{3+}/Ce^{4+} ratio for the Ag(5)_M-CeO_2 catalyst.

Consequently, since the surface Ce^{3+}/Ce^{4+} ratio and [V_O] are important factors that affects the generation of O_x^{n-}, the proper values of the Ce^{3+}/Ce^{4+} ratio and [V_O] are crucial for O_2^- generation and activity in soot oxidation [10,12,47]. This is because the excessive surface oxygen vacancies and Ce^{3+}/Ce^{4+} ratio could induce the formation of less active oxygen species rather than highly active O_2^- due to the further reduction of O_2 to O^- and O^{2-} species, resulting in the decrease of the catalysts' redox stability and activity [20,21,48,49]. However, on the other hand, if the [V_O] is too low, the total O_x^{n-} generation process will be decreased, resulting in reduced soot oxidation activity [21]. Hence, there should be a proper [V_O] value range that balances the activity and formation rate of O_x^{n-}, and the appropriate [V_O] may enhance the catalytic activity. Considering the Raman analysis results in Fig. 9, it is reasonable to suggest that the excessive values of Ce^{3+} ratio and [V_O] induced the generation of O^- and O^{2-} rather than O_2^-. As listed in Table 1, Ag(2)_M-CeO_2, Ag(10)_M-CeO_2, and Ag(20)_M-CeO_2 catalysts represented relatively higher Ce^{3+}/Ce^{4+} ratios and [V_O] than the Ag(5)_M-CeO_2. These inappropriate values for the Ce^{3+} ratio

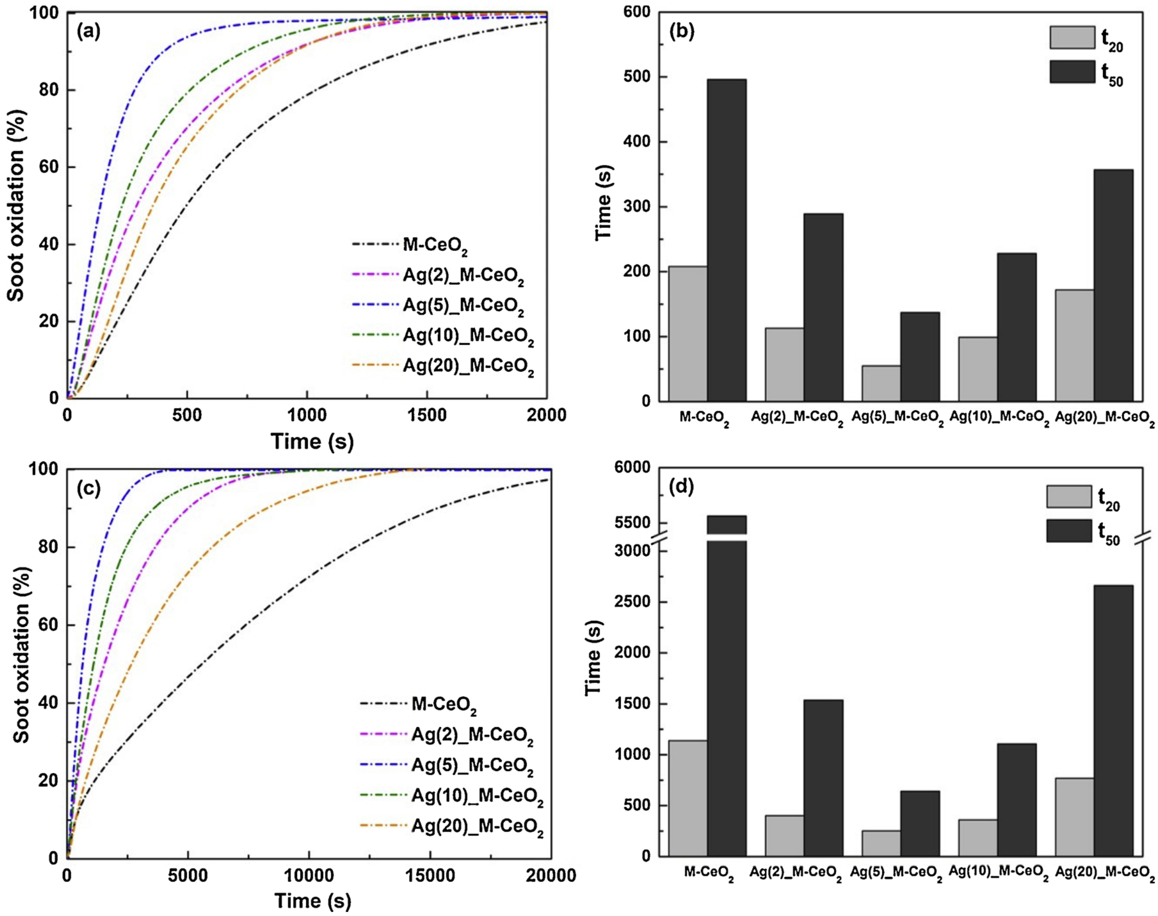

Fig. 7. The performance of soot oxidation over M-CeO_2 and Ag(x)_M-CeO_2 catalysts for isothermal conditions under loose contact. (a) soot oxidation over time, and (b) t_{20} and t_{50} of each catalyst at 500 °C; (c) soot oxidation over time, and (d) t_{20} and t_{50} of each catalyst at 450 °C. Reaction conditions: He (80 ml min^{-1}), O_2 (20 ml min^{-1}), H_2O (5 vol.%), catalyst/soot = 10/1.

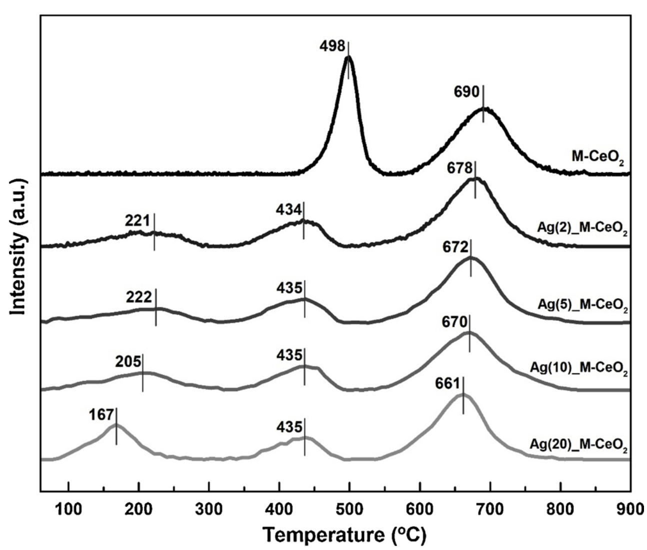

Fig. 8. H_2-TPR profiles of the M-CeO_2 and Ag(x)_M-CeO_2 catalysts.

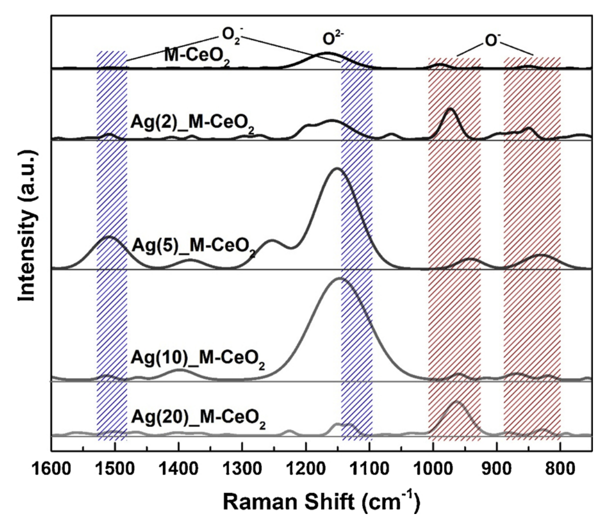

Fig. 9. Raman spectra of the M-CeO_2 and Ag(x)_M-CeO_2 catalysts.

and [V_O] may in turn hinder the generation of highly active oxygen species and lead to lower activity. Therefore, although Ag incorporation improved the activity of the catalysts, the proper amount of Ag is a significant factor in the effective generation of O_2^- over O^- and O^{2-}. When considering the results of the activity tests for soot oxidation, Ag (5)_M-CeO_2 could be a catalyst with the optimum amount of Ag for the generation of O_2^- with proper [V_O] among all Ag(x)_M-CeO_2 tested.

The correlation between the catalytic properties and activity difference is shown in Fig. 11. The various amounts of Ag on catalysts lead to different ratios of O_x^{n-} (Fig. 9) and levels of soot oxidation activity, which are mainly derived from the surface Ce^{3+}/Ce^{4+} ratio and [V_O]. More specifically, the activity of Ag(5)_M-CeO_2 catalysts with the appropriate Ce^{3+}/Ce^{4+} ratio and [V_O] was greatly improved due to enhanced generation of O_2^-, whereas the larger [V_O] of Ag(10)_M-CeO_2 induced less generation of O_2^- species and showed lower activity. In

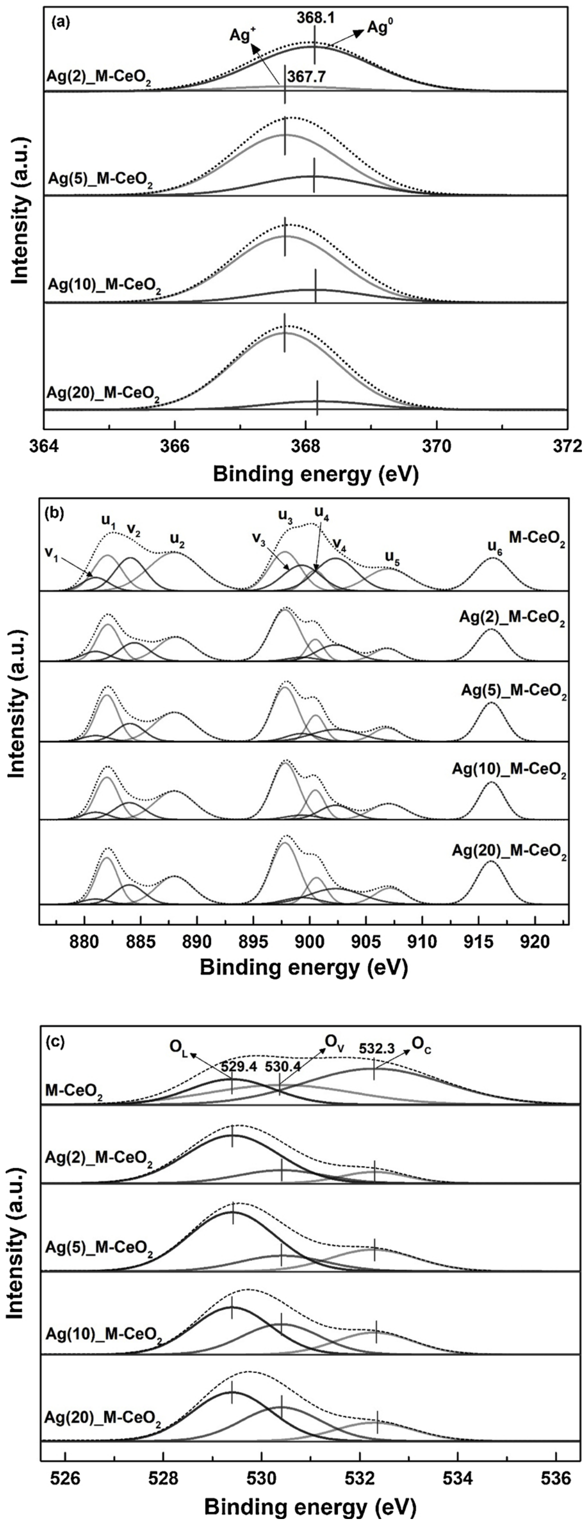

Fig. 10. XPS spectra of (a) Ag $3d_{5/2}$, (b) Ce 3d, and (c) O 1s for the M-CeO_2 and Ag(x)_M-CeO_2 catalysts.

contrast, Ag(2)_M-CeO_2 and Ag(20)_M-CeO_2 with inappropriate values of Ce^{3+}/Ce^{4+} and [O_V] promoted the generation of O^- species and O^{2-} rather than O_2^-. Hence, it should be noted that an appropriate amount of Ag on the CeO_2 is a considerably important factor in determining the catalytic activity since it influences the Ce^{3+}/Ce^{4+} ratio and [O_V] and induces the generation of O_x^{n-}, resulting in an increase of the soot oxidation catalytic activity.

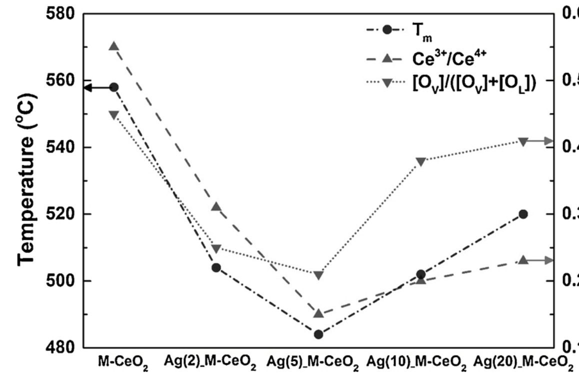

Fig. 11. Plots of T_m for soot oxidation (20 vol.% of O_2), Ce^{3+}/Ce^{4+} ratio, and $[O_V]/([O_V] + [O_L])$ ratio of the catalysts.

4. Conclusion

This study shows that macroporous CeO_2 (M-CeO_2) demonstrates improved activity in soot oxidation when compared to mesoporous CeO_2 catalyst. This is because the enlarged pore size of the M-CeO_2 catalyst could make soot particles pass through into the inner pore of the catalyst easily, and consequently overall contact between catalyst and soot was increased. With the Ag incorporation, Ag(x)_M-CeO_2 showed enhanced soot oxidation activity in all Ag loading amounts (2–20 wt.%). Especially, the Ag(5)_M-CeO_2 catalyst demonstrated higher soot oxidation activity than other catalysts, and the Raman spectra showed that the various catalytic performances of the Ag(x)_M-CeO_2 catalysts are due to differences in their ability to generate O_x^{n-}. The proper amount of Ag incorporation and metallic Ag could facilitate oxygen activation and promote the generation of highly active oxygen species through the reduction of atomic oxygen by surface oxygen vacancies. In contrast, an excessive Ce^{3+}/Ce^{4+} ratio and [V_O] of the catalyst induced the generation of less active oxygen species (O^- and O^{2-}) rather than O_2^-, which is an important factor greatly affecting the soot oxidation ability. Based on the above results, it was concluded that the appropriate amount of Ag incorporation on CeO_2 catalysts with a suitable macroporous structure is crucial in promoting the generation of O_2^- and improving the activity of catalysts for soot oxidation.

Acknowledgement

This work was supported by the National Research Foundation of Korea (NRF) grant funded by the Korea government (MSIP) (NRF-2016R1A5A1009592).

References

[1] N.D. Wasalathanthri, T.M. SantaMaria, D.A. Kriz, S.L. Dissanayake, C.-H. Kuo, S. Biswas, S.L. Suib, Mesoporous manganese oxides for NO_2 assisted catalytic soot oxidation, Appl. Catal. B 201 (2017) 543–551.
[2] M. Skaf, S. Aouad, S. Hany, R. Cousin, E. Abi-Aad, A. Aboukaïs, Physicochemical characterization and catalytic performance of 10% Ag/CeO_2 catalysts prepared by impregnation and deposition–precipitation, J. Catal. 320 (2014) 137–146.
[3] J.-H. Park, H. Noh, T.-S. Chang, C.-H. Shin, Low-temperature CO oxidation of Pt/$Al_{0.1}Ce_{0.9}O_x$ catalysts: Effects of supports prepared with different precipitants, Korean J. Chem. Eng. 35 (2018) 645–653.
[4] D.-W. Lee, J.Y. Sung, J.H. Park, Y.-K. Hong, S.H. Lee, S.-H. Oh, K.-Y. Lee, The enhancement of low-temperature combustion of diesel PM through concerted application of FBC and perovskite, Catal. Today 157 (2010) 432–435.
[5] Y.-K. Hong, D.-W. Lee, Y.-C. Ko, L. Yinghua, H.-S. Han, K.-Y. Lee, Passive NOx reduction with CO using Pd/TiO_2/Al_2O_3 + WGSR catalysts under simulated post-Euro IV diesel exhaust conditions, Catal. Lett. 136 (2010) 106–115.
[6] J.-H. Ryu, D.-H. Jeong, C. Bae-Hyeock, D.-W. Lee, K.-Y. Lee, H.-S. Lee, K.M. Chun, Experimental Study on DeNOx Performance by Plasma-catalyst (Ag, Au/Al_2O_3) System, SAE Tech. Pap. (2002).
[7] D.-W. Lee, J.Y. Sung, K.-Y. Lee, Combustion of diesel particulate matters under mixed catalyst system of fuel-borne catalyst and perovskite: influence of composition of perovskite ($La_{1-x}A'_xBO_3$: A' = K, Sr: 0 ≤ x ≤ 1; B = Fe, Cr, Mn) on combustion activity, Korean Chem. Eng. Res. (HWAHAK KONGHAK) 56 (2018)

281–290.
[8] B.M.V. Twigg, P.R. Phillips, Cleaning the air we breathe-controlling diesel particulate emissions from passenger cars, Platinum Metals Rev. 53 (2009) 27–34.
[9] M. Machida, Y. Murata, K. Kishikawa, D. Zhang, K. Ikeue, On the reasons for high activity of CeO_2 catalyst for soot oxidation, Chem. Mater. 20 (2008) 4489–4494.
[10] A. Bueno-López, Diesel soot combustion ceria catalysts, Appl. Catal. B 146 (2014) 1–11.
[11] P. Doggali, S. Kusaba, Y. Teraoka, P. Chankapure, S. Rayalu, N. Labhsetwar, $La_{0.9}Ba_{0.1}CoO_3$ perovskite type catalysts for the control of CO and PM emissions, Catal. Commun. 11 (2010) 665–669.
[12] L. Shuang, W. Xiaodong, W. Duan, R. Rui, Ceria-based catalysts for soot oxidation: a review, J. Rare Earths 33 (2015) 567–590.
[13] A. Bueno-L˘pez, K. Krishna, M. Makkee, J.A. Moulijn, Active oxygen from CeO_2 and its role in catalysed soot oxidation, Catal. Lett. 99 (2005) 203–205.
[14] I. Atribak, An. Bueno-López, A. García-García, Thermally stable ceria–zirconia catalysts for soot oxidation by O_2, Catal. Commun. 9 (2008) 250–255.
[15] A. Trovarelli, Catalytic properties of ceria and CeO_2-containing materials, Catal. Rev. 38 (1996) 439–520.
[16] K. Krishna, A. Bueno-López, M. Makkee, J. Moulijn, Potential rare earth modified CeO_2 catalysts for soot oxidation: I. Characterisation and catalytic activity with O_2, Appl. Catal. B 75 (2007) 189–200.
[17] G. Zhang, Z. Zhao, J. Liu, G. Jiang, A. Duan, J. Zheng, S. Chen, R. Zhou, Three dimensionally ordered macroporous $Ce_{1-x}Zr_xO_2$ solid solutions for diesel soot combustion, Chem. Commun. 46 (2010) 457–459.
[18] A. Setiabudi, J. Chen, G. Mul, M. Makkee, J.A. Moulijn, CeO_2 catalysed soot oxidation: the role of active oxygen to accelerate the oxidation conversion, Appl. Catal. B 51 (2004) 9–19.
[19] S. Jelles, B. Van Setten, M. Makkee, J. Moulijn, Molten salts as promising catalysts for oxidation of diesel soot: importance of experimental conditions in testing procedures, Appl. Catal. B 21 (1999) 35–49.
[20] S. Liu, X. Wu, W. Liu, W. Chen, R. Ran, M. Li, D. Weng, Soot oxidation over CeO_2 and Ag/CeO_2: factors determining the catalyst activity and stability during reaction, J. Catal. 337 (2016) 188–198.
[21] H. Wang, S. Liu, Z. Zhao, X. Zou, M. Liu, W. Liu, X. Wu, D. Weng, Activation and deactivation of Ag/CeO_2 during soot oxidation: influences of interfacial ceria reduction, Catal. Sci. Technol. 7 (2017) 2129–2139.
[22] K. Yamazaki, T. Kayama, F. Dong, H. Shinjoh, A mechanistic study on soot oxidation over CeO_2–Ag catalyst with 'rice-ball'morphology, J. Catal. 282 (2011) 289–298.
[23] K. Yamazaki, Y. Sakakibara, F. Dong, H. Shinjoh, The remote oxidation of soot separated by ash deposits via silver–ceria composite catalysts, Appl. Catal. A 476 (2014) 113–120.
[24] E. Aneggi, J. Llorca, C. de Leitenburg, G. Dolcetti, A. Trovarelli, Soot combustion over silver-supported catalysts, Appl. Catal. B 91 (2009) 489–498.
[25] L. Murrell, R. Carlin, Silver on ceria: an example of a highly active surface phase oxide carbon oxidation catalyst, J. Catal. 159 (1996) 479–490.
[26] K.-i. Shimizu, H. Kawachi, A. Satsuma, Study of active sites and mechanism for soot oxidation by silver-loaded ceria catalyst, Appl. Catal. B 96 (2010) 169–175.
[27] M. Piumetti, S. Bensaid, N. Russo, D. Fino, Nanostructured ceria-based catalysts for soot combustion: investigations on the surface sensitivity, Appl. Catal. B 165 (2015) 742–751.
[28] L. Wang, S. Fang, N. Feng, H. Wan, G. Guan, Efficient catalytic removal of diesel soot over Mg substituted $K/La_{0.8}Ce_{0.2}CoO_3$ perovskites with large surface areas, Chem. Eng. J. 293 (2016) 68–74.
[29] Y. Wei, Z. Zhao, J. Liu, S. Liu, C. Xu, A. Duan, G. Jiang, Multifunctional catalysts of three-dimensionally ordered macroporous oxide-supported Au@ Pt core–shell nanoparticles with high catalytic activity and stability for soot oxidation, J. Catal. 317 (2014) 62–74.
[30] J. Xu, J. Liu, Z. Zhao, C. Xu, J. Zheng, A. Duan, G. Jiang, Easy synthesis of three-dimensionally ordered macroporous $La_{1-x}K_xCoO_3$ catalysts and their high activities for the catalytic combustion of soot, J. Catal. 282 (2011) 1–12.
[31] J.P. Bosco, K. Sasaki, M. Sadakane, W. Ueda, J.G. Chen, Synthesis and characterization of three-dimensionally ordered macroporous (3DOM) tungsten carbide: application to direct methanol fuel cells, Chem. Mater. 22 (2009) 966–973.
[32] Y. Wei, J. Liu, Z. Zhao, Y. Chen, C. Xu, A. Duan, G. Jiang, H. He, Highly active catalysts of gold nanoparticles supported on three-dimensionally ordered macroporous $LaFeO_3$ for soot oxidation, Angew. Chem. 50 (2011) 2326–2329.
[33] J. Xu, J. Liu, Z. Zhao, J. Zheng, G. Zhang, A. Duan, G. Jiang, Three-dimensionally ordered macroporous $LaCo_xFe_{1-x}O_3$ perovskite-type complex oxide catalysts for diesel soot combustion, Catal. Today 153 (2010) 136–142.
[34] G. Bergeret, P. Gallezot, Particle size and dispersion measurements, Handbook of Heterogeneous Catalysis: Online, (2008), pp. 738–765.
[35] J. Zheng, J. Liu, Z. Zhao, J. Xu, A. Duan, G. Jiang, The synthesis and catalytic performances of three-dimensionally ordered macroporous perovskite-type $LaMn_{1-x}Fe_xO_3$ complex oxide catalysts with different pore diameters for diesel soot combustion, Catal. Today 191 (2012) 146–153.
[36] H. Yan, C.F. Blanford, B.T. Holland, W.H. Smyrl, A. Stein, General synthesis of periodic macroporous solids by templated salt precipitation and chemical conversion, Chem. Mater. 12 (2000) 1134–1141.
[37] Z. Qu, F. Yu, X. Zhang, Y. Wang, J. Gao, Support effects on the structure and catalytic activity of mesoporous Ag/CeO_2 catalysts for CO oxidation, Chem. Eng. J. 229 (2013) 522–532.
[38] E.J. Lee, J.W. Lee, J. Lee, H.-K. Min, J. Yi, I.K. Song, D.H. Kim, Ag-(Mo-W)/ZrO_2 catalysts for the production of propylene oxide: effect of pH in the preparation of ZrO_2 support, Catal. Commun. 111 (2018) 80–83.
[39] L. Ma, D. Wang, J. Li, B. Bai, L. Fu, Y. Li, Ag/CeO_2 nanospheres: efficient catalysts for formaldehyde oxidation, Appl. Catal. B 148 (2014) 36–43.
[40] B. Liu, C. Li, Y. Zhang, Y. Liu, W. Hu, Q. Wang, L. Han, J. Zhang, Investigation of catalytic mechanism of formaldehyde oxidation over three-dimensionally ordered macroporous Au/CeO_2 catalyst, Appl. Catal. B 111 (2012) 467–475.
[41] E. Aneggi, D. Wiater, C. de Leitenburg, J. Llorca, A. Trovarelli, Shape-dependent activity of ceria in soot combustion, ACS Catal. 4 (2013) 172–181.
[42] T. Tabakova, F. Boccuzzi, M. Manzoli, J. Sobczak, V. Idakiev, D. Andreeva, A comparative study of nanosized IB/ceria catalysts for low-temperature water-gas shift reaction, Appl. Catal. A 298 (2006) 127–143.
[43] H. Zhang, A. Zhu, X. Wang, Y. Wang, C. Shi, Catalytic performance of Ag–Co/CeO_2 catalyst in NO–CO and NO–CO–O_2 system, Catal. Commun. 8 (2007) 612–618.
[44] Y. Kang, M. Sun, A. Li, Studies of the catalytic oxidation of CO over Ag/CeO_2 catalyst, Catal. Lett. 142 (2012) 1498–1504.
[45] V.V. Pushkarev, V.I. Kovalchuk, J.L. d'Itri, Probing defect sites on the CeO_2 surface with dioxygen, J. Phys. Chem. B 108 (2004) 5341–5348.
[46] Y. Choi, H. Abernathy, H.T. Chen, M. Lin, M. Liu, Characterization of O_2–CeO_2 interactions using in situ Raman spectroscopy and first-principle calculations, Chem. Phys. Chem. 7 (2006) 1957–1963.
[47] Y. Li, Y. Du, Y. Wei, Z. Zhao, B. Jin, X. Zhang, J. Liu, Catalysts of 3D ordered macroporous ZrO_2-supported core–shell Pt@CeO_{2-x} nanoparticles: effect of the optimized Pt–CeO_2 interface on improving the catalytic activity and stability of soot oxidation, Catal. Sci. Technol. 7 (2017) 968–981.
[48] S. Liu, X. Wu, J. Tang, P. Cui, X. Jiang, C. Chang, W. Liu, Y. Gao, M. Li, D. Weng, An exploration of soot oxidation over CeO_2-ZrO_2 nanocubes: do more surface oxygen vacancies benefit the reaction? Catal. Today 281 (2017) 454–459.
[49] Y. Gao, A. Duan, S. Liu, X. Wu, W. Liu, M. Li, S. Chen, X. Wang, D. Weng, Study of Ag/$Ce_xNd_{1-x}O_2$ nanocubes as soot oxidation catalysts for gasoline particulate filters: balancing catalyst activity and stability by Nd doping, Appl. Catal. B 203 (2017) 116–126.